Ground-state characterizations of systems predicted to exhibit $L1_1$ or $L1_3$ crystal structures

Lance J. Nelson and Gus L. W. Hart
Department of Physics and Astronomy, Brigham Young University, Provo, Utah 84602, USA

Stefano Curtarolo
Department of Mechanical Engineering and Materials Science, Duke University, Durham, North Carolina 27708, USA

(Received 15 August 2011; revised manuscript received 15 December 2011; published 8 February 2012)

Despite their geometric simplicity, the crystal structures $L1_1$ (CuPt) and $L1_3$ ($CdPt_3$) do not appear as ground states experimentally, except in Cu-Pt. We investigate the possibility that these phases are ground states in other binary intermetallic systems, but overlooked experimentally. Via the synergy between high-throughput and cluster-expansion computational methods, we conduct a thorough search for systems that may exhibit these phases and calculate order-disorder transition temperatures when they are predicted. High-throughput calculations predict $L1_1$ ground states in the systems Ag-Pd, Ag-Pt, Cu-Pt, Pd-Pt, Li-Pd, Li-Pt, and $L1_3$ ground states in the systems Cd-Pt, Cu-Pt, Pd-Pt, Li-Pd, Li-Pt. Cluster expansions confirm the appearance of these ground states in some cases. In the other cases, cluster expansion predicts unsuspected derivative superstructures as ground states. The order-disorder transition temperatures for all $L1_1/L1_3$ ground states were found to be sufficiently high that their physical manifestation may be possible.

DOI: 10.1103/PhysRevB.85.054203 PACS number(s): 61.66.Dk, 31.15.A−, 81.30.Bx

I. INTRODUCTION

A scan of experimentally observed binary metallic phases shows that some appear many times. For example, the familiar prototypes CuAu and Cu_3Au (*Strukturbericht* $L1_0$ and $L1_2$, respectively) are found in experimental phase diagrams 51 and 294 times, respectively.[1] This is contrasted by the single occurrence of two other simple phases: Cu-Pt (*Strukturbericht* $L1_1$), and a 3:1 phase reported in the Cu-Pt system referred to as $L1_1^+$ by Müller *et al.*, which we will refer to as $L1_3$.[2,3] All four structures are among the simplest possible fcc-derived superstructures, with four atoms per cell or fewer.

Many frequently observed crystal structures are fcc-derived superstructures. The atoms in these crystals all lie on fcc lattice sites.[4] There are 17 fcc-derived superstructures with four atoms per cell or fewer.[5] Among them are some commonly observed crystal structures: $L1_0$, $L1_2$, $MoPt_2$, $D0_{22}$, C6, and $C11_b$. Other structures in this group, including $L1_1$ and $L1_3$, are essentially missing from experimental phase diagrams.

One way to assess the likelihood of a particular structure's physical manifestation is through a geometric comparison. When atom-atom correlations deviate significantly from the correlations of a random configuration, that structure is more likely to occur. Such "nonrandom" structures have energies much greater than or much less than the random alloy, with the latter ones competing for ground-state status.

This idea was used to assigned a likelihood value to all fcc-derived superstructures up to four atoms per cell.[5] $L1_0$ was found to be most likely and $L1_2$ was ranked number 4 in the list. $L1_1$ came in just below $L1_2$, and $L1_3$ was found to be slightly less likely than $D0_{22}$, which appears 19 times in experimental phase diagrams, and is slightly more likely than $MoPt_2$, which appears 10 times in experimental phase diagrams.

Will the $L1_1$ and $L1_3$ structures appear in systems other than Cu-Pt? If so, in which systems will they occur and how can we identify those alloys? Well-known empirical methods, such as the Hume-Rothery rules[6] and Pettifor-type structure maps,[7] are one way to predict thermodynamically stable phases and miscibility behavior. These methods analyze experimental data and attempt to establish phase stability trends. Pettifor maps, for example, group together all occurrences of a given structure into well-defined domains, thus helping one to make educated guesses as to what other systems may exhibit the same phase. These methods have their utility and successes, but provide little insight where experimental data are scarce or lacking completely.

In contrast, *ab initio* high-throughput methods scan a large database of possible ground states exploring a larger space than other heuristic methods. Furthermore, such high-throughput data can be used to construct lattice-based models, which can be used to search over large portions of configuration space. Combining these methods increases the search space beyond what each method can do separately.[8]

Our goal is to uncover new occurrences of the phases $L1_1$ and $L1_3$ by combining the strengths of these two computational techniques. $L1_1$ and $L1_3$ phases have only been observed experimentally in the Cu-Pt system.[2,9] However, both phases were predicted to exist in the Ag-Pd system,[10] and $L1_3$ was predicted to be stable in Pd-Pt and Cd-Pt using a first-principles-based data-mining technique.[11,12]

II. HIGH THROUGHPUT

The high-throughput (HT) approach combines heuristic information with first-principles calculations to predict stable phases. In this method, prior knowledge of experimentally observed phases is used to build a database of candidate ground states. First-principles calculations are then performed on all structures in the database and for all possible binary systems. In this way, the power of prior knowledge is combined with the precision and accuracy of first-principles calculations. Currently, our binary alloy HT database contains calculations for over 630 systems, a total of ∼150 000 calculations available in the AFLOWLIB consortium repository.[13]

First-principles calculations were performed within the framework of AFLOW,[8,11,12,14–18] which employs the VASP software for computing energies.[19] Projector-augmented-wave (PAW) potentials were used and exchange-correlation functionals parametrized by Perdew, Burke, and Ernzerhof under the generalized gradient approximation (GGA).[20–22] A dense k-mesh scheme was used to perform the numeric integration over the Brillioun zone.[23] Optimal choices of the unit cells, by standardization of the reciprocal lattice, were adopted to accelerate the convergence of the calculations.[17,18]

The effect of spin-orbit coupling has not been included in our calculations because of the following consideration. In Ref. 24, we found that the inclusion of relativistic spin-orbit coupling in transition-metal alloys affects the total energies but leaves differences between competing phases essentially the same. The issue can be understood if one considers that most of the spin-orbit coupling energy comes from core electrons, which are not shared in the highly delocalized metallic bond responsible for the formation energy. Thus, the relativistic contribution to the total energy in the space of concentrations is a linear combination of energies, a simple tilt of the whole convex hull, which does not alter, by construction, the thermodynamic competition between phases.

This data-mining technique explores a large number of candidate ground states, but it only explores the space of (almost) all *known* alloy structures. The method will successfully find the ground states among a pool of contenders, but can not rule out new, unexpected structures. To find the unexpected ground states, we need a way to rapidly explore more configurations.

To do this, we consider essentially all derivative superstructures of the parent lattices. All possible derivative superstructures are enumerated,[25,26] then the energies of all enumerated structures are compared to find the ground states. Typically, the number of superstructures enumerated is large (millions) to ensure that we find the global minima. Due to the computational cost, direct first-principles calculation of all enumerated superstructures is not possible. For this reason, a model Hamiltonian must be used to compute their energies.

III. CLUSTER EXPANSION

A useful model Hamiltonian for lattice configuration problems is the cluster expansion (CE). The CE can be used to quickly compute the energies of a large number of configurations. Here, we give a brief review of the CE methodology.[27–29]

The CE expresses a material's physical property as a linear combination of geometric figures or "clusters." In the CE formalism, an atomic configuration is defined by first assigning a spin value for each atomic type. The configurational property of an atomic configuration is then expressed by first averaging over spin products, something typically referred to as *correlation functions*. These correlation functions form a basis by which a material's physical properties can be expanded:

$$E(\vec{\sigma}) = J_0 + \sum_f \sum_1^{N_f} \Pi_f(\vec{\sigma}) J_f,$$

where $\vec{\sigma}$ characterizes the atomic occupancy on the lattice, $\Pi_f(\vec{\sigma})$ represents the averaged spin products over cluster f for configuration $\vec{\sigma}$. The J_n's are the expansion coefficients and N_f is the number of clusters of type f.

These coefficients are found by fitting the CE to a set of training data, typically first-principles energies of a small group of structures. A genetic algorithm is then used to fit the training data to the CE.[30,31] The CE predictions are iteratively verified, adding to the set of training data as needed.[32] When combined with enumeration algorithms,[25,26] the resulting CE can calculate the energies of millions of derivative structures with near first-principles accuracy in a few minutes.

Training-data calculations were performed using the VASP software. We used PAW potentials and exchange-correlation functionals parametrized by Perdew, Burke, and Ernzerhof under the generalized gradient approximation.[20–22] An equivalent k-mesh scheme was used for Brillioun-zone integration to reduce systematic error.[33]

The CE can compute the energy of atomic configurations in large cells very fast, making it possible to perform thermodynamic Monte Carlo (MC) simulations. These simulations require millions of energy calculations and would not be possible without a fast Hamiltonian such as the CE.

IV. RESULTS

As mentioned previously, the current HT database contains data for over 630 binary systems. This database was searched for occurrences of $L1_1$ and $L1_3$ ground states. $L1_1$ was found to be a ground state in the following systems: Ag-Pd, Ag-Pt, Cu-Pt, and Pd-Pt. $L1_3$ was found in Cd-Pt, Cu-Pt, Pd-Pt, Li-Pd, Li-Pt, and Ag-Pd.

Cluster expansions were constructed for all of these systems. CE training data consisted of $\sim$100 first-principles calculations. Any new ground states predicted by the CE were verified by first principles and added to the input set. The process of fitting to the training data, performing a ground-state search, and adding any new ground-state predictions to the training-data set was iterated many times to ensure convergence of the CE.

In the figures that follow, several hundred first-principles calculations are shown. These structures were selected for calculation either as part of the initial training-data set, or because the CE predicted them as ground states at some point during the iterative procedure explained above. By verifying all ground-state predictions with first-principles calculations, and making them available as training data, the CE is slowly refined to predict more accurately and more completely cover configuration space.

Ground-state searches were performed by calculating the energies of all structures up to 16 atoms per cell. Rarely are structures with >12 atoms per cell seen in the experimental literature. By expanding the search well beyond this, we are ensured that searches are essentially exhaustive. Converged cluster expansions were used to perform MC simulations for determining order-disorder transition temperatures.

In what follows, we give a short summary of our results for each system studied. Some reported ground states do not have a *Strukturbericht* designation or an experimental prototype because they have never been observed. We will refer to these structures using a number that represents

their location in our enumerated list. A full crystallographic description of these structures can be found in the Supplemental Material.[34] Additionally, this crystallographic information can be generated using our enumeration code, which is available via SOURCEFORGE.[39]

A. Ag-Pd

Experimental reports for this system are scarce. It is reported to be a solid solution from the solidus line down to 900 °C, with no reports of ordered phases appearing.[35–38] First-principles results predict eight ordered phases in this system (see Fig. 1).

Ag-Pd system

Composition (% Pd)	Experiment (Refs. 35–38)	HT (Ref. 13)	CE
12.5	Solid solution >900 ° C	Ca_7Ge	**fcc-154685*** **Ca_7Ge*** ∼0.9 meV/atom above fcc-154685
18.75	Solid solution >900 ° C	Two-phase	**fcc-154665***
∼21.5	Solid solution	Two-phase	**fcc-33781***
25	Solid solution >900 ° C	$D0_{23}$	**$D0_{24}$*** **$D0_{23}$*** ∼0.7 meV/atom above $D0_{24}$
31.125	Solid solution >900 ° C	Two-phase	**fcc-154439***
33	Solid solution >900 ° C	**C37***	Two-phase
37.5	Solid solution >900 ° C	Two-phase	**fcc-154395***
∼ 42	Solid solution	Two-phase	**fcc-18195***
40	Solid solution	f-55	Two-phase
50	Solid solution >900 ° C	$L1_1$	Two-phase D_4 ∼1.1 meV/atom above tie line
	>900 ° C		$L1_1$ ∼1.2 meV/atom above tie line
∼57	Solid solution >900 ° C	Two-phase	**fcc-25645***
75	Solid solution >900 ° C	$L1_3$	Two-phase $L1_3$ ∼3.7 meV/atom above tie line

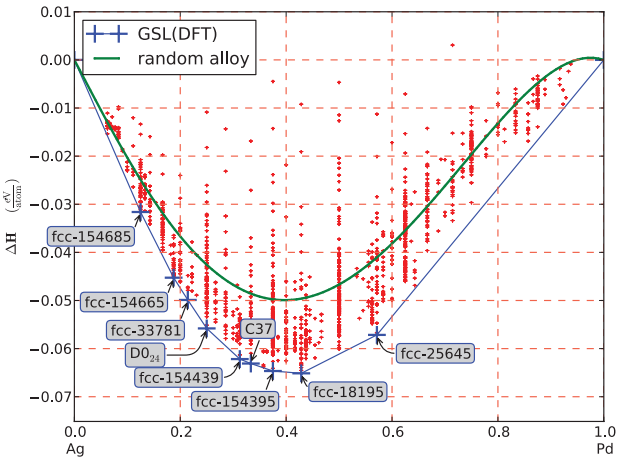

FIG. 1. (Color online) Low-temperature ground states for the binary system Ag-Pd as determined by the combined effort of HT and CE. The other curve shows the energy of the random alloy as computed by the CE. Crystal structures listed above the plot that are in bold and with an asterisk next to them indicate ground states.

On the Ag-rich side, the first-principles phases Ag_7Pd (Ca_7Ge), Ag_3Pd ($D0_{23}$), and Ag_3Pd ($D0_{24}$) are found to be ground states, all of which are well-known experimental phases. The formation energies of $D0_{23}$ and $D0_{24}$ differ by less than 1 meV/atom (within numerical accuracy) and thus we report both as the ground state. At composition Ag_7Pd, we also find an fcc-derived phase (fcc-154685, oS32, #63), the formation energy of which is found to be within 1 meV/atom of the Ca_7Ge structure.

Other first-principles phases on the Ag-rich side found using cluster-expansion searches are $Ag_{13}Pd_3$ (fcc-154665, oS32, #67), $Ag_{11}Pd_3$ (fcc-33781, mS28, #12), $Ag_{11}Pd_5$ (fcc-154439, oS32, #21), $Ag_{10}Pd_6$ (fcc-154395, oS32, #66), and Ag_8Pd_6 (fcc-18195, #15). The ordered phase Ag_3Pd (C37) was found by HT to be ∼1 meV/atom lower than the CE tie line.

On the Pd-rich side, the first-principles phase at composition Ag_6Pd_8 is stable. At composition 1:1, we find a two-phase region with $L1_1$ and D_4 being ∼1 meV/atom above the tie line. Similarly, at composition $AgPd_3$, we find a two-phase region, with $AgPd_3$ ($L1_3$) appearing ∼3.7 meV/atom above the tie line. Thus, the low-temperature stable phases predicted here by CE are somewhat different than what has been previously predicted[10]; notably, the presence of $L1_1$ and $L1_3$ as low-temperature ground states is not confirmed.

The difference in formation energy between the tie line and the $L1_1$ structure is arguably within the limits of numerical accuracy. It is possible that AgPd ($L1_1$) is a ground state in this system. Furthermore, the atom-atom correlations of the two structures at the breaking points of the tie line at ∼42 at.% and ∼57 at.% were found to be very similar to $L1_1$, indicating the system may prefer $L1_1$-like configurations.

Thermodynamic MC performed at 42 at.% Pd found a transition temperature of about −70 °C. This low transition temperature explains why no ordered phases have been observed experimentally.

B. Pd-Pt

Phase diagrams derived from experimental studies show this system to be phase separating (see Fig. 2).[35,36,40–42] However, a recent experimental study by Lang *et al.* found the system to be miscible at these temperatures, although no ordered phases were reported. Lang reported the kinetics of this system to be prohibitively slow, probably due to the similarity of Pd and Pt.

Computational results reveal a handful of ordered phases, but the ground states predicted by HT and CE differ over the entire composition range, with no single phase being predicted as a ground state by both methods. HT calculations find the following stable ordered phases at low temperatures: Pd_3Pt ($L1_3$), PtPt ($L1_1$), $PdPt_3$ ($L1_2$), and $PdPt_7$ (Ca_7Ge).[11]

CE ground-state searches reveal a different set of ground states, all at different compositions than the HT ground states. There are four phases with monoclinic symmetry at compositions $Pd_{10}Pt_4$, Pd_4Pt_3, Pd_3Pt_4, and Pd_4Pt_{10}. There is one phase at composition Pd_2Pt_{14} with orthorhombic symmetry and one phase at composition $Pd_{13}Pt_1$ with orthorhombic symmetry. Since these phases have never been seen in any binary system, they were not a part of the HT database.

Pd-Pt system

Comp. % Pt	Experiment (Refs.35,36,40–42)	HT (Ref. 13)	CE
∼7	Two-phas	Two-phase	**fcc-34368***
25	Two-phase	$L1_3$	Two-phase
∼28	Two-phas	Two-phase	**fcc-33153***
∼42	Two-phas	Two-phase	**fcc-177***
50	Two-phase	$L1_1$ (CuPt)	Two-phase
∼57	Two-phas	Two-phase	**fcc-159***
∼71	Two-phas	Two-phase	**fcc-16988***
75	Two-phase	$L1_2$ $L1_3$∼1.4 meV/atom above $L1_2$	Two-phase
87.5	Two-phase	Ca_7Ge	**fcc-160466***

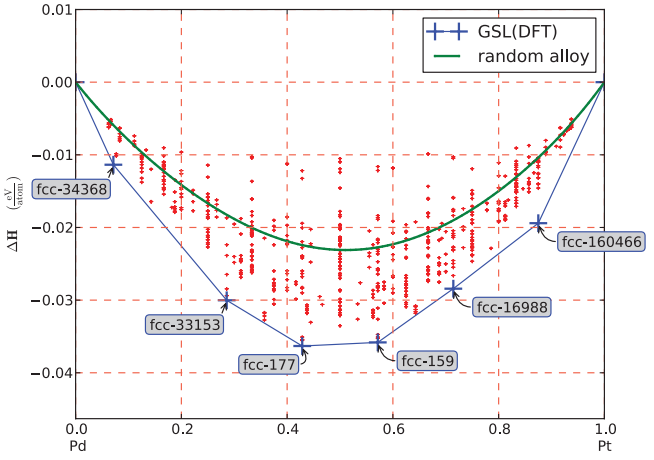

FIG. 2. (Color online) Low temperature ground states for the binary system Pd-Pt as determined by the combined effort of HT and CE. All stable phases found by the CE are unsuspected and therefore not predicted by HT. Metallurgical challenges may prevent these unsuspected phases from being seen experimentally. The other curve shows the energy of the random alloy as computed by the CE. Crystal structures listed above the plot that are in bold and with an asterisk next to them indicate ground states.

Thermodynamic MC performed at 42 at.% Pt found a transition temperature of ∼25 °C. This low transition temperature, no doubt a result of the slow kinetics reported by Lang *et al.*, explains why no ordered phases have been observed experimentally.

C. Li-Pd

The phase diagram for this system is mostly known, reporting five ordered phases of known structure and one compound of unknown structure.[35,36,43,44] For Li-rich compositions, the experimental phases $Li_{15}Pd_4$ ($Cu_{15}Si_4$), Li_2Pd (Hg_2U), and LiPd (B_h) are ground states. One experimental phase of unknown character is reported at composition Li_6Pd. The stability of LiPd (B_h) is confirmed by first principles to be stable at low temperatures. Other first-principles phases found to be stable in this region are Li_8Pd_2 (hcp-982, mP10, #11), Li_3Pd ($D0_3$), and Li_2Pd (bcc-9, hP3, #164), as shown in Fig. 3.

Pd-rich ground states reported experimentally are $Li_{1.37}Pd_{2.63}$ (mP4, #10) and $LiPd_7$ (Ca_7Ge). First-principles ground states for this region are Li_3Pd_5 (fcc-625, cF32, #166), $LiPd_3$ ($L1_3$), and $LiPd_7$ (Ca_7Ge), confirming the stability of the experimental phase $LiPd_7$ (Ca_7Ge) down to low temperatures.

Li-Pd system

Composition (% Pd)	Experiment (Refs.35,36,43,44)	HT (Ref. 13)	CE
16–17	UOP	Two-phase	Two-phase
20	$Cu_{15}Si_4$	$D1_a$ ($MoNi_4$)	**hcp-982*** bcc-53 ∼0.4 meV/atom above hcp-982 $D1_a$ ∼ 3 meV/atom above hcp-982
25	Two-phase	$D0_3$	**$D0_3$*** $D0_a$(Cu_3Ti) ∼1 meV/atom above $D0_3$ $D0_{22}$(Al_3Ti) ∼5 meV/atom above $D0_3$
33.3	Hg_2U	C49 ($ZrSi_2$)	**bcc-9*** hcp-44 ∼1 meV/atom above bcc-9 $MoPt_2$ ∼2 meV/atom above bcc-9
45–52	B_h (WC)	B_h (WC)	**B_h (WC)** * $L1_1$ ∼4 meV/atom above B_h
62.5	Two-phase	Two-phase	**fcc-625***
60–71	$Li_{1.37}Pd_{2.63}$	Two-phase	Two-phase
75	Two-phase	$L1_3$($CdPt_3$)	**$L1_3$($CdPt_3$)***
87.5	Ca_7Ge	Ca_7Ge	**Ca_7Ge***

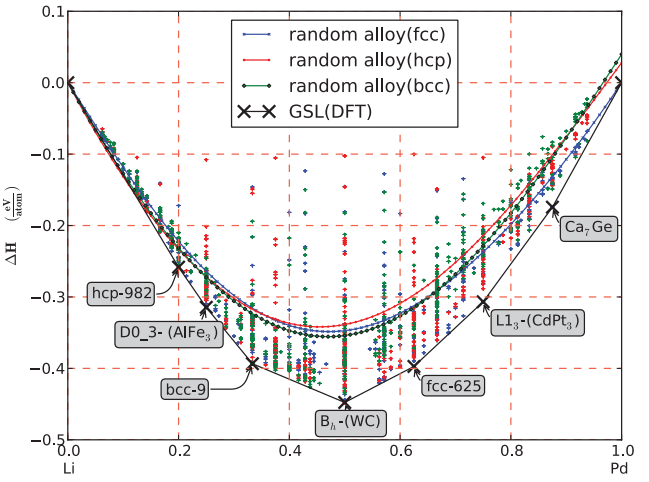

FIG. 3. (Color online) Low-temperature ground states for the binary system Li-Pd as determined by the combined effort of HT and CE. $L1_3$ appears as a ground state in this system as well as two unsuspected Li-rich phases (hcp-982 and bcc-9) and one unsuspected Pd-rich phase (fcc-625). The other curves show the energy of the random alloy for the different lattices considered by CE methods. Crystal structures listed above the plot that are in bold and with an asterisk next to them indicate ground states. UOP designates the unknown ordered phase.

The first-principles ground states Li_8Pd_2 (hcp-982, mP10, #11), Li_2Pd (bcc-9, hP3, #164), and Li_3Pd_5 (fcc-625, cF32, #166) were found by CE ground-state searches. These phases have never been reported in any binary system, and as such were not included in the HT database.

MC simulations performed at composition $LiPd_3$ find the transition temperature for $LiPd_3$ ($L1_3$) to be 900 °C, making this system a good candidate for finding another occurrence of $L1_3$.

D. Li-Pt

Phase diagrams show three known and two unknown compounds appearing in the Li-Pt system.[35,36,45] (see Fig. 4.) For Li-rich compositions, experiment reports two unknown

Li-Pt system

Composition (% Pt)	Experiment (Refs.35,36,45)	HT (Ref. 13)	CE
16.6	UOP	Two-phase	Two-phase
20	UOP	$D1_a$ ($MoNi_4$)	**hcp-982*** $D1_a$ ∼5 meV/atom above hcp-982
33.3	Two-phase	**C32***	hcp-60 fcc-116/bcc-117 ∼ 9 meV/atom above hcp-60 $MoPt_2$∼10 meV/atom above hcp-60
50	B_h (WC)	B_h (WC)	**L1₁*** **B_h (WC)*** ∼1 meV/atom above $L1_1$
62.5	Two-phase	Two-phase	**fcc-625***
66–73	$MgCu_2$	Two-phase	Two-phase
75	Two-phase	$L1_3$	**$L1_3$***
87.5	Ca_7Ge	Ca_7Ge	**Ca_7Ge***

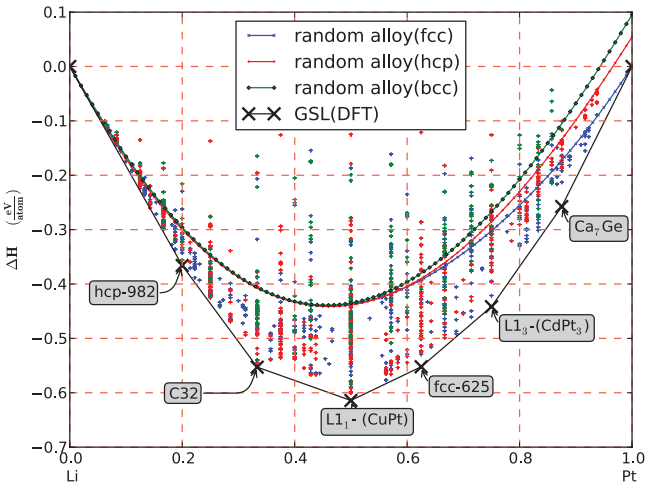

FIG. 4. (Color online) Low-temperature ground states for the binary system Li-Pt as determined by the combined effort of HT and CE. $L1_3$ appears as a ground state in this system as well as one unsuspected Li-rich phase (hcp-982) and one unsuspected Pd-rich phase (fcc-625). The other curves show the energy of the random alloy for the different lattices considered by CE methods. Crystal structures listed above the plot that are in bold and with an asterisk next to them indicate ground states. UOP designates the unknown ordered phase.

structures at stoichiometry: Li_5Pt and Li_4Pt. At composition Li_4Pt, the first-principles ground state Li_4Pt (hcp-982, mP10, #11) is predicted. No first-principles ground states are found at composition Li_5Pt, instead we predict the two-phase region $Li \leftrightarrow Li_4Pt$ (hcp-982, mP10, #11). The first-principles ground state Li_2Pt (C32) is predicted by HT data. Its formation energy is ∼4 meV/atom lower than the first-principles phase Li_2Pt (hcp-60, mS12, #15) found by CE. The stability of LiPt (B_h) down to $T = 0$ K is confirmed by first-principles data, with LiPt ($L1_1$) being degenerately stable with it (difference in formation energy within numerical accuracy).

For Pt-rich compositions, the experimental ground states $LiPt_2$ ($MgCu_2$) and $LiPt_7$ (Ca_7Ge) are reported. $LiPt_7$ (Ca_7Ge) is confirmed to be stable in the low-temperature regime by first-principles calculations. The experimental phase at composition $LiPt_2$ is not stable at $T = 0$ K according to first-principles data. Other first-principles ground states for this region are Li_3Pt_5 (fcc-625, cF32, #166) and $LiPt_3$ ($L1_3$).

The first-principles ground state with structure C32 was not considered by CE searches because it is not a derivative superstructure. HT databases included C32, and found it as a ground state in this system, because it was suspected as a ground state, having been observed in other binary systems. The first-principles ground states Li_4Pt (hcp-982, mP10, #11) and Li_3Pt_5 (fcc-625, cF32, #166) were found by CE searches and not considered by HT due to it being unsuspected to occur based on experimental data.

MC simulations performed at composition $LiPt_3$ find the transition temperature for $LiPt_3$ ($L1_3$) to be 1450 °C. This makes this system a good candidate for finding another occurrence of $L1_3$.

E. Cu-Pt

There are five experimentally reported ground states in this system and one unidentified phase reported[2,9,35,36,46–51] (see Fig. 5). Experimentally reported Cu-rich phases include Cu_3Pt ($L1_2$) and an unknown phase at composition Cu_3Pt. The phase with the $L1_2$ structure is reported to have composition range of stability extending from 10 at.% Pt to 25 at.% Pt. However, experimental reports include no x-ray analysis, and therefore

Cu-Pt system

Composition (% Pt)	Experiment (Refs.2,9,35,36, 46–51)	HT (Ref. 13)	CE
12.5	$L1_2(Cu_3Au)$	Ca_7Ge	**Ca_7Ge***
16.6	$L1_2(Cu_3Au)$	Two-phase	**fcc-10848***
25	$L1_2(Cu_3Au)$	$D0_{23}(Al_3Zr)$	**$D0^*_{24}$** $D0_{23}$ ∼ 2.3 meV/atom above $D0_{24}$ $L1_2$ ∼ 14 meV/atom above $D0_{24}$
23–28	UOP	Two-phase	Two-phase
35–54	$L1_1$(CuPt)	$L1_1$(CuPt)	**$L1_1$(CuPt)***
62–68	Cu_3Pt_5	Two-phase	**fcc-625***
65–75	$L1_3(CdPt_3)$	$L1_3(CdPt_3)$	**$L1_3$ ($CdPt_3$)***
70–79	Ca_7Ge	Ca_7Ge	**Ca_7Ge***

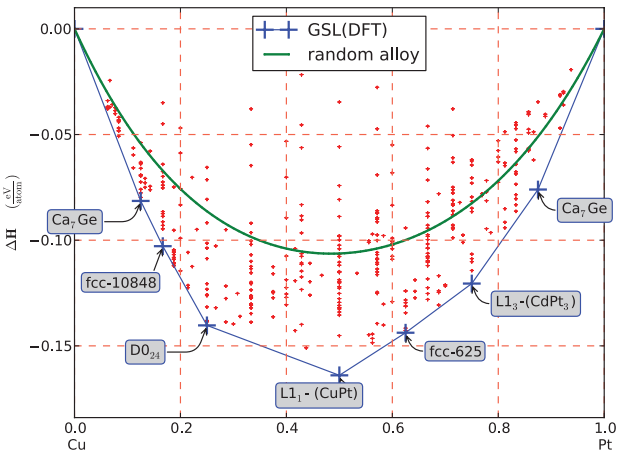

FIG. 5. (Color online) Low-temperature ground states for the binary system Cu-Pt as determined by the combined effort of HT and CE. The low-temperature regime at Cu-rich composition is characterized by three phases not previously observed. One other unsuspected phase is found at Pt-rich composition (fcc-625). The other curve shows the energy of the random alloy as computed by the CE. Crystal structures listed above the plot that are in bold and with an asterisk next to them indicate ground states. UOP designates the unknown ordered phase.

merely conjecture that the stable phase is the $L1_2$ structure. First-principles ground states found in this composition region were Cu_7Pt (Ca_7Ge), $Cu_{10}Pt_2$ (fcc-10848, hP12, #164), and Cu_3Pt ($D0_{24}$). Thus, the experimental phase Cu_3Pt ($L1_2$) does not continue to be stable down to low temperatures. The unidentified experimental phase reported at composition Cu_3Pt is not stable at low temperature according to first-principles data, instead we find the two-phase region Cu_3Pt ($D0_{24}$) $\leftrightarrow$ CuPt ($L1_1$).

For Pt-rich compositions, the experimental phases Cu_3Pt_5, $CuPt_3$ ($L1_3$), and $CuPt_7$ (Ca_7Ge) are reported. The experimental phase at composition Cu_3Pt_5 was reported to have rhombohedral symmetry, but the existence of this phase has not been confirmed by additional studies. First-principles calculations confirm the stability of $CuPt_3$ ($L1_3$) and $CuPt_7$ (Ca_7Ge) at low temperature and find Cu_3Pt_5 (fcc-625, cF32, #166), which has trigonal symmetry, to be stable at composition 3:5. A transition from the trigonal phase to the rhombohedral phase may occur at higher temperatures.

The first-principles ground states Cu_3Pt_5 (fcc-625, cF32, #166) and $Cu_{10}Pt_2$ (fcc-10848, hP12, #164) are derivative superstructures and were found to be ground states using CE ground-state searches. These crystal structures have not been observed in any binary alloy and were not included in the HT database.

First-principles calculations confirm the stability of CuPt ($L1_1$) down to $T = 0$ K. Monte Carlo simulations performed at 1:1 stoichiometry indicate a phase transition occurring at ~450 °C, which is in disagreement with the experimentally reported temperature of ~800 °C.

Ag-Pt system

Composition (% Pt)	Experiment (Refs.35,36,50, 52–56)	HT (Ref. 13)	CE
12.5	Two-phase	Ca_7Ge	Two-phase **Ca_7Ge*** ~1.3 meV/atom above tie line
25	$L1_2$ (Cu_3Au)	Two-phase	Two-phase
33	Two-phase	Two-phase	**fcc-8***
40	Two-phase	f-38	Two-phase
42–45	UOP	Two-phase	Two-phase
47–52	UOP	$L1_1$(CuPt)	**$L1_1$(CuPt)***
69–81	UOP	Two-phase	Two-phase

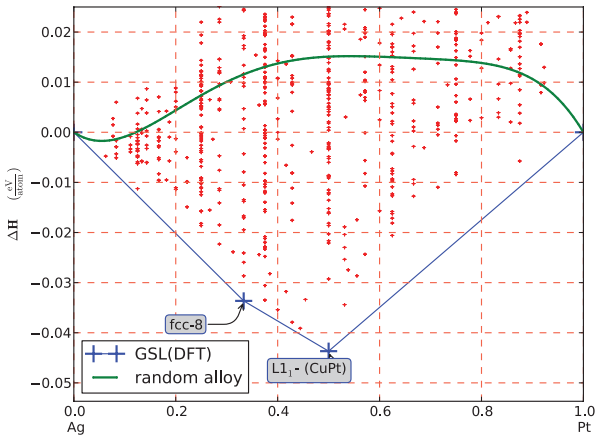

FIG. 6. (Color online) Low-temperature ground states for the binary system Ag-Pt as determined by the combined effort of HT and CE. AgPt ($L1_1$) is a low-temperature ground state for this system. The other curve shows the energy of the random alloy as computed by the CE. Crystal structures listed above the plot that are in bold and with an asterisk next to them indicate ground states. UOP designates the unknown ordered phase.

F. Ag-Pt

Phase diagrams derived from experimental studies indicate three unidentified phases appearing at composition $Ag_{55}Pt_{45}$, AgPt, and $AgPt_3$. Additionally, the experimental phase Ag_3Pt ($L1_2$) is reported[35,36,50,52–56] (see Fig. 6).

First-principles ground states found for this system differ from the experimental phases mentioned. Ag_2Pt (fcc-8, hP3, #164) and AgPt ($L1_1$) are found to be stable by first-principles methods. The phase with structure fcc-8 is an AB2 stacking in the [111] direction of a fcc lattice. Ag_7Pt (Ca_7Ge) was found to be ~1.3 meV/atom above the tie line. This small difference is within numerical accuracy, and thus we report it as a ground state as well.

In 1996, Durussel and Feschotte proposed a new phase diagram, reporting an ordered phase appearing at composition $Ag_{15}Pt_{17}$ and rejecting all other ordered phases for this system.[56] The new phase was reported to be fcc based with a cubic unit cell appearing at ~800 °C. A full crystallographic characterization of this reported phase was not given.

The CE constructed for this system was used in an attempt to find a phase with the reported properties. Instead of enumerating all possible 32-atom unit cells, we used a new enumeration algorithm to only enumerate the ones at 15:17 stoichiometry with cubic unit cells.[57] This greatly reduced the time needed to enumerate and the size of the structure list.

Searching the 32 atoms/cell configurations yielded no ground state at 15:17 stoichiometry. However, the 32-atom cell with the lowest formation energy was very $L1_1$ like. We assume that the reported phase was in fact $L1_1$ with a small number of random defects, or that the experimental determination of the composition was incorrect.

MC simulation performed at composition 1:1 indicates a transition temperature of ~700 °C, which agrees nicely with the experimental transition temperature of the unknown ordered phase reported by Ref. 54 as well as the reported transition temperature of the supposed $Ag_{15}Pt_{17}$ phase reported by Durussel and Feschotte.[56]

G. Cd-Pt

Published phase diagrams derived from experiment show several ordered phases, giving information down to 100 °C on the Cd-rich side of the phase diagram and down to 500 °C on the Pt-rich side[35,36,58] (see Fig. 7). On the Cd-rich side, the experimental phase Cd_5Pt (# 215) and three unknown phases at composition Cd_3Pt, Cd_7Pt_3, and Cd_2Pt are reported. First-principles phases Cd_3Pt ($D0_{11}$) and Cd_2Pt (Hg_2Pt) are found to be stable in this composition range.

The three first-principles phases at composition $Cd_{14}Pt_2$, $Cd_{10}Pt_2$, and $Cd_{11}Pt_3$ were found by the CE but were removed from the tie line by the presence of the first-principles phases Cd_3Pt ($D0_{11}$) and Cd_2Pt (Hg_2Pt) found by HT. These crystal structures were beyond the applicability range of the CE since they are not derivative superstructures.

Cd-Pt system

Composition (% Pt)	Experiment (Refs.35,36,58)	HT (Refs.13)	CE
12.5	Two-phase	Two-phase	hcp-60823
16–18	Cd_5Pt	Two-phase	hcp-4898
21.5	Two-phase	Two-phase	hcp-14666
23–25	UOP	**$D0_{11}$***	$D0_a$
		$D0_a$	
26–28	UOP	Two-phase	Two-phase
31–38	UOP	**Hg_2Pt***	hcp-4852
51–59	$L1_0$(CuPt)	$L1_0$(CuPt)	**$L1_0$ (CuPt)***
68.75	Two-phase	Two-phase	**fcc-154897***
70–80	$L1_2$	$L1_3$	**$L1_3$***
			$L1_2 \sim 11$ meV/atom above $L1_3$
87.5		Ca_7Ge	**Ca_7Ge***

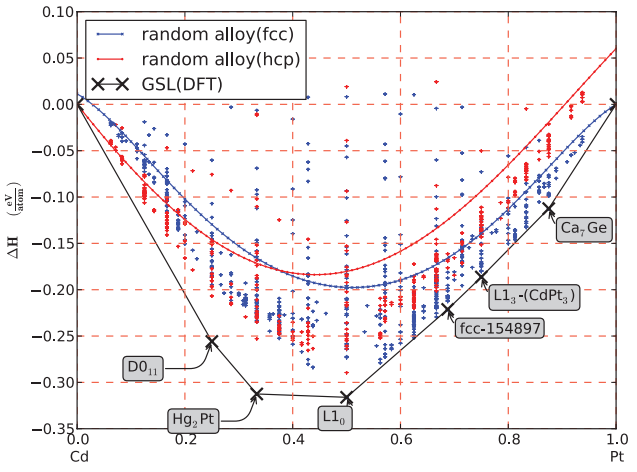

FIG. 7. (Color online) Ground-state crystal structures for the binary system Cd-Pt as determined by the combined effort of HT and CE. HT predictions dominate the Cd-rich portion of the phase diagram, with $D0_{11}$ and Hg_2Pt being the only stable Cd-rich phases. This system is predicted to exhibit the rarely seen phase $L1_3$ for Pt-rich composition. Crystal structures listed above the plot that are in bold and with an asterisk next to them indicate ground states. UOP designates the unknown ordered phase.

For Pt-rich compositions, experimental ground states are found at compositions 1:1 and 1:3 with structures $L1_0$ and $L1_2$, respectively. The stability of CdPt ($L1_0$) is verified by first-principles calculations, but the experimental phase $CdPt_3$ ($L1_2$) is replaced by the first-principles phase $CdPt_3$ ($L1_3$) as a ground state. Additionally, other first-principles phases found to be stable in this region are Cd_5Pt_{11} (fcc-154897, mS32, #12) and $CdPt_7$ (Ca_7Ge). The CE identified the first-principles phase Cd_5Pt_{11} (fcc-154897, mS32, #12) as stable.

The characterization of the Cd-rich portion of the phase diagram by HT, together with the identification of Cd_5Pt_{11} (fcc-154897, mS32, #12) as ground states by CE, demonstrates the synergy between these two methods. Either method working alone would not have been able to fully characterize the low-temperature phase diagram for this system.

Two MC simulations were carried out at $CdPt_3$ composition. The first started with perfect $L1_3$ at $T = 0$ and increased the temperature. The other MC simulation started out at high temperature and cooled down to $T = 0$. The former simulation shows $L1_3$ persisting up to ~700 °C followed by a transition to disorder. The latter simulation reveals a transition to $L1_2$ at ~700 °C, with no transition to $L1_3$ ever being observed. This suggests that a free energy barrier between $L1_2$ and $L1_3$ is preventing $L1_3$ from ordering at low temperature.

H. Pt-Zn

Phase diagrams report two well-known ordered phases in this system and one phase that is lesser known. Additionally, three unidentified phases are reported in this system.[35,36,59,60] (see Fig. 8). Experimental ground states include $L1_2$ (Cu_3Au) and $L1_0$ (CuAu), with the composition range of stability for $L1_0$ reported to be from 32–47 at.% Zn.

First-principles data confirm the stability of $L1_0$ (CuAu) down to the low-temperature regime. At composition Pt_3Zn, first-principles calculations indicate $L1_3$ ($CdPt_3$) to be stable, indicating that the phase with the $L1_2$ structure does not continue to be stable down to low temperatures.

Other first-principles ground states identified at Pt-rich compositions include Pt_7Zn (Ca_7Ge), $Pt_{10}Zn_2$ (fcc-10775, mS24, #12), and Pt_5Zn_3 (fcc-630, tI16, #139). The latter two phases were unsuspected derivative superstructures and were identified as ground states by the CE.

Pt-Zn system

Composition (% Pt)	Experiment (Refs.35,36,59, 60)	HT (Ref.13)	CE
12.5	Solid solution	Ca_7Ge	**Ca_7Ge***
16.6	Solid solution	Two-phase	**fcc-10775***
25	$L1_2$ (Cu_3Au)	$L1_3$ ($CdPt_3$)	**$L1_3$ ($CdPt_3$)***
			$L1_2 \sim 7$ meV/atom above $L1_3$
37.5	Two-phase	Two-phase	**fcc-630***
50	$L1_0$	$L1_0$	**$L1_0$***
62–63	UOP	Two-phase	Two-phase
66	Two-phase	C49	**fcc-77***
75	UOP	$D0_{22}$	**$D0_{22}$***
77–81	$Pt_{10.8}Zn_{36.2}$	Two-phase	Two-phase
83.3	Two-phase	Two-phase	**hcp-50***
87.5	Two-phase	Two-phase	**hcp-184***
≈88.8	UOP	Two-phase	Two-phase

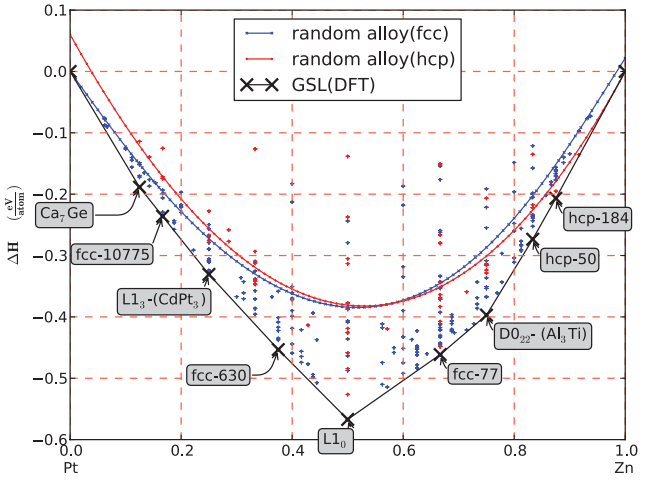

FIG. 8. (Color online) Low-temperature ground states for the binary system Pt-Zn as predicted by the combined effort of HT and CE. The phase with structure $L1_3$ is a low-temperature ground state for this system at composition Pt_3Zn. The other curves show the energies of the random alloys for the different lattices considered by CE method. Crystal structures listed above the plot that are in bold and with an asterisk next to them indicate ground states. UOP designates the unknown ordered phase.

For Zn-rich compositions, the experimental ground state $Pt_{10.8}Zn_{36.2}$ (cF392, #216) is reported, as well as three unidentified ground states at compositions $PtZn_{1.7}$, $PtZn_3$, and $PtZn_8$. At composition $PtZn_3$, first-principles data find the well-known experimental phase $PtZn_3$ ($D0_{22}$) to be stable. The presence of the other two unknown phases in the low-temperature regime is not confirmed by first-principles calculations. Other first-principles ground states with Zn-rich composition include Pt_2Zn_4 (fcc-77, oS12, #63), $PtZn_5$ (hcp-50, hR6, #155), and Pt_2Zn_4 (hcp-184, mS16, #5). These three phases are unsuspected, having never been seen in experimental phase diagrams, and were found by the CE.

Two MC simulations were carried out at Pt_3Zn composition. The first started with perfect $L1_3$ at $T = 0$ and increased the temperature. The other MC simulation started out at high temperature and cooled down to $T = 0$. The former simulation shows $L1_3$ persisting up to $\sim$1200 °C followed by a transition to disorder. The latter simulation reveals a transition to an unknown ordered phase, perhaps a mix of $L1_2$ and $L1_3$, at $\sim$1200 °C, with no transition to $L1_3$ ever being observed. This suggests that a free energy barrier is preventing $L1_3$ from ordering at low temperature.

V. CONCLUSIONS

A. Summary of $L1_1/L1_3$ predictions

HT and CE techniques have been used to characterize the low-temperature ground states for several binary systems that may exhibit the rarely seen phases $L1_1$ and $L1_3$. In some cases, these phases were identified as ground states. Specifically, we predict $L1_1$ to be stable in Ag-Pt, Cu-Pt, and Li-Pt. We also predict $L1_3$ to be stable in Li-Pd, Li-Pt, Cu-Pt, Cd-Pt, and Pt-Zn.

For other systems, cluster-expansion-guided ground-state searches found other low-energy crystal structures, which superseded $L1_1$ and/or $L1_3$ on the convex hull. This was exemplified in the Pd-Pt and Ag-Pd systems where CE finds a whole host of unsuspected ground states. In these systems, the predicted ground states were unsuspected derivative superstructures, and thus not included in the HT database.

Conversely, HT found ground states that were outside the applicability range of the CE. For example, in the Cd-Pt system HT found $D0_{11}$ and Hg_2Pt, which are not derivative superstructures. The presence of these two ground states lowered the convex hull below all of the CE-predicted Cd-rich ground states. The combined use of HT and CE helps us to characterize the low-temperature ground states of these systems more thoroughly and accurately than we could have done with either method by itself.

B. Summary of differences between experiment and theory

Differences between experimental reports and computational predictions are exhibited in each system. Some systems, such as Ag-Pd and Pd-Pt, are reported to be phase separating or noncompound forming by experiment, but are predicted by computation to have stable ordered phases. These systems are instances where computation can direct future experimental efforts to find new ordered phases.

Other systems, such as Li-Pd, Li-Pt, and Ag-Pt, are reported to exhibit ordered compounds of known or unknown character, but computational predictions differ somewhat. For example, in Li-Pd and Li-Pt, $L1_3$ is predicted to be stable by computation for Pt/Pd-rich concentrations. Experimental reports, on the other hand, show a two-phase region at this stoichiometry for both systems. Similar differences occur in Li-rich Li-Pt/Pd and in Ag-Pt.

In Cd-Pt and Cu-Pt, the reported appearance of $L1_2$ differs from the first-principles prediction of $L1_3$. However, a closer look at the experimental work reveals no convincing evidence for the appearance of the $L1_2$ phase. In these systems, experimentalists merely surmise the stability of the $L1_2$ structure. On the other hand, the CE-predicted $L1_3$ structure does not appear during cool-down MC simulations either, possibly suggesting a free energy barrier between the high-temperature phase and the $L1_3$ structure.

Even when convincing crystallographic evidence for a phase's appearance is given, as in Pt_3Zn ($L1_2$), a first-principles-based prediction, which differs from experiment, does not constitute a contradiction with experiment. Metallurgical and kinetic challenges prevent experiments from reporting about phase stability at temperatures lower than a few hundred degrees Celsius at best. This leaves gaps in phase diagrams, gaps which first-principles studies seek to fill.

Any differences between experimental reports and computational predictions are usually attributable to either (1) the addition of entropy at finite temperature, which stabilizes disorder or a phase different from the $T = 0$ phase, or (2) slow kinetics, which can prevent the predicted phase from forming below its predicted transition temperature. We hope that our work will serve as motivation for future experimental work to find the predicted phases.

C. Noticeable trends

The results presented here indicate that the phase with structure $L1_3$ seems to only appear in Pt/Pd-rich alloys, which could indicate that these elements are important for this crystal structure to form. The unsuspected derivative superstructure (fcc-625, cF32, #166) appeared in three systems: Li-Pd, Li-Pt, and Cu-Pt, possibly indicating that this crystal structure may appear more broadly and thus should be added to the HT database.

ACKNOWLEDGMENTS

We thank W. Setyawan for fruitful discussions. Research was supported by NSF (Grants No. NDMR-0908753 and No. DMR-0639822) and ONR (Grants No. N00014-11-1-0136 and No. N00014-09-1-0921). We are grateful for extensive use of the Fulton Supercomputing Center at Brigham Young University and Teragrid resources (MCA-07S005).

[1]M. Sluiter, Phase Transitions **80**, 299 (2007).
[2]R. Miida and D. Watanabe, J. Appl. Crystallogr. **7**, 50 (1974).
[3]G. L. W. Hart, Phys. Rev. B **80**, 014106 (2009).
[4]Due to atomic and cell relaxation, the atoms may not lie precisely on the lattice sites. However, the experimental structure can be readily associated with the ideal enumerated structure. The energy associated with the relaxation is accounted for implicitly by the CE.
[5]G. L. W. Hart, Nat. Mater. **6**, 941 (2007).
[6]W. Hume-Rothery, *The Metallic State* (Clarendon, Oxford, 1931).
[7]D. Pettifor, J. Phys. C: Solid State Phys. **3**, 367 (1970).
[8]O. Levy, G. L. W. Hart, and S. Curtarolo, J. Am. Chem. Soc. **132**, 4830 (2010).
[9]N. S. Kurnakow and W. A. Nemilow, Z. Anorg. Allg. Chem. **210**, 1 (1933).
[10]S. Müller and A. Zunger, Phys. Rev. Lett. **87**, 165502 (2001).
[11]S. Curtarolo, D. Morgan, and G. Ceder, CALPHAD: Comput. Coupling Phase Diagrams Thermochem. **29**, 163 (2005).
[12]S. Curtarolo, D. Morgan, K. Persson, J. Rodgers, and G. Ceder, Phys. Rev. Lett. **91**, 135503 (2003).
[13]S. Curtarolo, W. Setyawan, R. H. Taylor, S. Wang, J. Xue, K. Yang, G. L. W. Hart, S. Sanvito, M. Buongiorno Nardelli, N. Mingo, and O. Levy (unpublished).
[14]O. Levy, R. V. Chepulskii, G. L. W. Hart, and S. Curtarolo, J. Am. Chem. Soc. **132**, 833 (2010).
[15]O. Levy, G. L. W. Hart, and S. Curtarolo, Acta Mater. **58**, 2887 (2010).
[16]R. Taylor, S. Curtarolo, and G. L. W. Hart, J. Am. Chem. Soc. **132**, 6851 (2010).
[17]W. Setyawan and S. Curtarolo, Comput. Mater. Sci. **49**, 299 (2010).
[18]W. Setyawan, R. M. Gaume, S. Lam, R. S. Feigelson, and S. Curtarolo, ACS Comb. Sci. **13**, 382 (2011).
[19]G. Kresse and J. Hafner, Phys. Rev. B **47**, 558 (1993).
[20]G. Kresse and D. Joubert, Phys. Rev. B **59**, 1758 (1999).
[21]G. Kresse and J. Furthmüller, Comput. Mater. Sci. **6**, 15 (1996).
[22]P. E. Blöchl, Phys. Rev. B **50**, 17953 (1994).
[23]H. Monkhorst and J. Pack, Phys. Rev. B **13**, 5188 (1976).
[24]O. Levy, G. L. W. Hart, and S. Curtarolo, Acta Mater. **58**, 2887 (2010).
[25]G. L. W. Hart and R. W. Forcade, Phys. Rev. B **77**, 224115 (2008).
[26]G. L. W. Hart and R. W. Forcade, Phys. Rev. B **80**, 014120 (2009).
[27]J. Sanchez, F. Ducastelle, and D. Gratias, Phys. A (Amsterdam) **128**, 334 (1984).
[28]D. Fontaine, Solid State Phys. **47**, 33 (1994).
[29]A. Zunger, *First-Principles Statistical Mechanics of Semiconductor Alloys and Intermetallic Compounds* (NATO Advanced Study Institute, New York, 1994), pp. 361–419.
[30]V. Blum, G. L. W. Hart, M. J. Walorski, and A. Zunger, Phys. Rev. B **72**, 165113 (2005).
[31]D. Lerch, O. Wieckhorst, G. L. W. Hart, R. W. Forcade, and S. Müller, Modell. Simul. Mater. Sci. Eng. **17**, 055003 (2009).
[32]V. Blum and A. Zunger, Phys. Rev. B **70**, 155108 (2004).
[33]S. Froyen, Phys. Rev. B **39**, 3168 (1989).
[34]See Supplemental Material at http://link.aps.org/supplemental/10.1103/PhysRevB.85.054203 for a full crystallographic description of these structures.
[35]T. Massalski, H. Okamoto, P. Subramanian, L. Kacprzak, and W. Scott, *Binary Alloy Phase Diagrams* (American Society for Metals, Metals Park, OH, 1986), Vol. 1.
[36]P. Villars, M. Berndt, K. Brandenburg, K. Cenzual, J. Daams, F. Hulliger, T. Massalski, H. Okamoto, K. Osaki, and A. Prince, J. Alloys Compd. **367**, 293 (2004).
[37]R. Ruer, Z. Anorgan. Chem. **51**, 315 (1906).
[38]E. Savitskii and N. Pravoverov, Russ. J. Inorg. Chem. **6**, 253 (1961).
[39]A complete description of this crystal structure can be generated using the enumeration code, which is freely available for download via SOURCEFORGE: [http://sourceforge.net/projects/enum/].
[40]S. R. Bharadwaj, A. S. Kerkar, S. N. Tripathi, and S. R. Dharwadkar, J. Less-Commom Met. **169**, 167 (1991).
[41]S. R. Bharadwaj and S. N. Tripathi, J. Alloy Phase Diagrams **6**, 118 (1990).
[42]G. M. Kuznetsov, E. I. Rytvin, V. A. Nikonova, I. V. adn Mazurov, B. S. Drilenok, and L. A. Sportsmen, Russ. Metall. (Engl. Transl.) **4**, 189 (1985).
[43]R. Howard, CALPHAD: Comput. Coupling Phase Diagrams Thermochem. **14**, 1 (1990).
[44]O. J. Loebich and C. J. Raub, J. Less-Common Met. **55**, 67 (1977).
[45]O. J. Loebich and C. Raub, J. Less-Common Met. **70**, 47 (1980).
[46]E. W. Collins, R. D. Smith, and J. C. Ho, J. Less-Common Met. **46**, 189 (1976).
[47]S. Ogawa, H. Iwasaki, and A. Terada, J. Phys. Soc. Jpn. **34**, 384 (1973).
[48]R. S. Frani and R. W. Cahn, J. Mater. Sci. **8**, 1453 (1973).
[49]L. R. Bidwell, W. J. Sghulz, and R. K. Saxer, Acta Metall. **15**, 1143 (1967).
[50]F. Doerinckel, Z. Anorgan. Chem. **54**, 333 (1907).
[51]A. Schneider and U. Esch, Z. Electrochem. Angew. Physik. Chem. **50**, 290 (1944).
[52]H. Ebert, J. Abart, and J. Voitlander, J. Less-Common Met. **91**, 89 (1983).
[53]W. J. Klement and H. Luo, IEEE Trans. Metall. Sci. **227**, 1253 (1963).
[54]A. Schneider and U. Esch, Z. Electrochem. Angew. Physik. Chem. **49**, 72 (1943).
[55]C. H. Johansson and J. O. Linde, Ann. Phys. (NY) **6**, 458 (1930).
[56]P. Durussel and P. Feschotte, J. Alloys Compd. **239**, 226 (1996).
[57]G. L. W. Hart, L. J. Nelson, and R. W. Forcade (unpublished).
[58]H. Nowotny, E. Bauer, A. Stempfl, and H. Bittner, Monatsh. Chem. **83**, 221 (1952).
[59]Y. Khan, B. V. R. Murty, and K. Schubert, J. Less-Common Met. **21**, 293 (1970).
[60]H. Nowotny, E. Bauer, A. Stempfl, and H. Bittner, Monatsh. Chem. **83**, 221 (1952).